

Journal of Materials Chemistry C

Accepted Manuscript



This is an *Accepted Manuscript*, which has been through the Royal Society of Chemistry peer review process and has been accepted for publication.

Accepted Manuscripts are published online shortly after acceptance, before technical editing, formatting and proof reading. Using this free service, authors can make their results available to the community, in citable form, before we publish the edited article. We will replace this *Accepted Manuscript* with the edited and formatted *Advance Article* as soon as it is available.

You can find more information about *Accepted Manuscripts* in the [Information for Authors](#).

Please note that technical editing may introduce minor changes to the text and/or graphics, which may alter content. The journal's standard [Terms & Conditions](#) and the [Ethical guidelines](#) still apply. In no event shall the Royal Society of Chemistry be held responsible for any errors or omissions in this *Accepted Manuscript* or any consequences arising from the use of any information it contains.

A Highly Conductive, Flexible Transparent Composite Electrode Based on the Lamination of Silver nanowires and Polyvinyl Alcohol

Xin He*, Ruihui He, A'lei Liu, Xiangyuan Chen, Zhilong Zhao, Sheng Feng, Ning Chen and Mei Zhang

School of Applied Physics and Materials, Wuyi University, Jiangmen 529020, People's Republic China

In this study, a spin-coating method was demonstrated for producing silver nanowire films on flexible polyethylene terephthalate substrates. To improve the inherent, poor uniformity in conductivity and lower high surface roughness of silver nanowire films, a composite film based on silver nanowire network and polyvinyl alcohol was fabricated by a mechanical lamination technique. The effects of mechanical pressure and laminating time on the photoelectric characterizations of the composite films were investigated. Stable electrical channels of silver nanowire network were established on the substrate by laminating the composite layers using a pressure of 30 MPa for 10 min. Transmittance of 86.9% at wavelength of 550 nm with sheet resistance of 0.75 Ω /sq and haze of 7.1% were measured for the silver nanowires-polyvinyl alcohol film. Furthermore, the composite film also showed low surface roughness, stable conductivity after 300 bending cycles, as well as the improved weak adhesion of nanowires to the substrate due to the compact contact between silver nanowires and polyvinyl alcohol.

Introduction

Over the last decade, there has been a continuing acceleration in the sales of optoelectronic devices such as touch screens, electronic paper, liquid crystal displays (LCD), organic light emitting diodes (OLED) and solar cells^[1-10]. Consequently, the demand for transparent electrodes as the essential component in these devices has kept pace with this trend. As is well known, indium tin oxide (ITO) film with high transparency, conductivity and a large work function is the dominant material used for the transparent conductor^[11-13]. However, next generation electronics require transparent electrodes be flexible, low-cost and capable of large-scale fabrication. Further development of ITO has been limited primarily due to scarcity of supply and its brittle nature of this

* Corresponding author. Tel. +86 750 3296393; Fax: +86 750 3296400.
E-mail address: hexinwyu@126.com (X. He)

ceramic^[14-16]. Consequently, potential alternatives to ITO are being sought for the development of the next generation of flexible devices. Currently, alternative transparent conducting materials include conducting polymers^[17, 18], carbon nanotubes^[19, 20], graphene^[21, 22], as well as metal nanostructures^[23-40]. Among these materials, the metal nanostructured silver nanowires (NWs) is considered as the most promising candidate for the replacement of ITO owing to its excellent photoelectric performance, compatibility with flexible substrates and easy adaptation to large-scale fabrication^[28-40]. Several researchers have reported applications of silver NW transparent electrodes in thin-film solar cells^[29, 30], OLED^[8, 31], touch panel^[3], fuel cell^[32, 33] and stretchable electronics^[34, 35]. The performance of these optoelectronic devices is largely dependent on the characteristics of silver NW percolation network. Therefore, investigating how to further improve the performance of silver NWs-based transparent electrodes is needed to advance the state of the art. For instance, freshly prepared Ag NW films usually exhibit poor conductivity, inadequate consistency of conductivity, weak adhesion to substrates and high surface roughness. To improve the electrical performance of Ag NW electrodes, most workers have made great efforts, generally focused on two aspects. One of these is the use of very long Ag NWs to fabricate percolation networks with reduced NW numbers and inter-NW junctions. This approach can increase the transparency and decrease the electrical resistance of the films^[3, 36]. The other approach is to reduce the high resistance of the inter-NW junctions in the Ag NW electrodes. The junctions are usually fused together to reduce resistance using high temperature annealing^[37], but this is not compatible with heat-sensitive plastic substrates. There are several methods that preclude the thermal annealing process, such as mechanical pressing^[38], plasmonic laser nano-welding^[3, 39], nano-soldering^[40]. Ko's group has developed a novel hybrid approach using a AgNW-conducting polymer composite, the polymer assists mechanical joining at the nanowire junction by capillary force, leading to a great improvement in the conductivity of transparent film^[40].

Although there have been many reports on the improvement of conductivity for Ag NW transparent electrodes, the uniformity of conductivity in the Ag NW electrode is rarely discussed in literatures. Nevertheless, it is one of significant parameters to determine the future manufacture and performance of optoelectronic devices. In this work, we demonstrated a transparent conducting composite film composed of silver NWs and PVA fabricated using a lamination technique. The composite film was prepared at room temperature without using any high temperature annealing

process, showing compatibility with flexible polymer substrates. The laminated films exhibit high conductivity, low surface roughness, excellent mechanical stability, as well as an improvement in adhesion of NWs to substrates. Especially, we investigated the uniformity of the conductivity for the composite film in this work, and obtained a great improvement in comparison to Ag NW film. These improved performances make Ag NWs-PVA composite film an excellent flexible transparent electrode candidate for the replacement of ITO in high-performance optoelectronic devices.

Experimental Method

Synthesis of Long Ag NWs

Long Ag NWs were synthesized using a hydrothermal process. Typically, 1.5 mmol of silver nitrate and 2 mmol of glucose were dissolved in a beaker at room temperature. Then, 0.3 mmol ferric sulfate was added and magnetically stirred for several minutes yielding a light yellow solution. Following this, 4.5 g poly (vinyl pyrrolidone) (K30) was introduced into the solution. The homogeneously mixed solution was transferred to a Teflon autoclave of 100 mL capacity, which was sealed and heated at 180 °C for 6 h. The resulting precipitate that exhibited a gray-green color was rinsed with dilute nitric acid to effectively get rid of the oxide from the surface of the Ag NWs. The excess nitric acid was removed using ethanol by centrifugation. The product was kept in ethanol to obtain a long Ag NW dispersion.

Fabrication of Ag NWs-PVA Composite Electrode

Fig. 1A is a schematic illustration of the fabrication procedure of the Ag NWs-PVA composite electrode. Initially, the Ag NW dispersion was spun on a cleaned bare polyethylene terephthalate (PET) substrate at room temperature to obtain a uniform thin film of silver NW networks. The photoelectrical performance of Ag NW film was dependent on the concentration of Ag NW dispersion, spinning speed and time. A PVA thin film with the thickness of approximately 10 μm was deposited onto a second bare PET substrate via the spin-coating method, and PVA concentration was fixed at 0.01 g/mL. Subsequently, the finished Ag NW film was inverted and placed on the PVA film. The Ag NW network could be totally transferred onto the surface of the PVA film using an enough mechanical pressure. Before transferring, PVA film was pre-heated in an infrared drying oven for several minutes in order to soften the PVA and make the transfer of Ag NW networks easier. Finally, the upper PET substrate of the Ag NW film was naturally peeled off, and

the Ag NWs-PVA composite film could be well fabricated.

Characterization

The nanostructure of the composite film was characterized using an X-ray diffractometer (XRD) (X'pert Pro MFD) with a Cu K α radiation ($\lambda=1.54178 \text{ \AA}$). The surface morphologies of transparent films were observed using an optical microscope (BX51M, Olympus) and a field emission scanning electron microscope (FESEM) (NoVaTM Nano SEM 430, FEI). The surface roughness and topography of the films were observed using an atomic force microscope (AFM) (MicroNano SPM, Zhuolun) with a tapping mode. High resolution transmission electron microscope (HRTEM) measurements of Ag NWs were carried out with JEOL-2100F electron microscopes, and the selected area electron diffraction (SAED) was also conducted on this microscope to characterize the microstructure of NWs. The transmittances were recorded using a UV-Vis spectrophotometer (UV 2550, Shimadzu) and the reference spectrum was evaluated from the cleaned bare PET substrate. The resistances of the films were evaluated using a digital multimeter (VC890C+ Victor). The sheet resistances of the films were measured using a four-point probe system (SZ-82, SX), and the final values were averaged from nine representative points on the conductive films (the schematic drawing for the location of nine points is shown in Fig. S1). X-ray photoelectron spectroscopy (XPS) patterns were taken on an ESCALAB 250XI (Thermo Scientific) instrument using monochromatic Al K α radiation. To compensate for surface charges effects, binding energies were calibrated using the C1s hydrocarbon peak at 284.6 eV.

Results and Discussion

Fig. 1A illustrates the fabrication procedure of Ag NWs-PVA composite film. Ag NW network was successfully transferred onto the surface of the PVA film by a mechanical lamination technique. Fig. 1B shows a photograph of a composite film with transmittance of 85% at 550 nm, suggesting that the Ag NWs-PVA film was uniformly coated over the large area of the PET substrate. The film displays a little haze due to the intense light scattering caused by the silver NWs, but it is sufficiently transparent that a red flower below the film can be clearly seen. Fig. 1C displays an optical micrograph of the composite film with transmittance of 85% at 550 nm. The random meshes of NWs were observed over the area of the substrate indicating no significant bundling, and the lengths of NWs are up to several hundred micrometers. As Ko et al. reported^[3], the long metal

NWs can form an effective electron percolation network with superior photoelectrical performance than shorter ones.

Fig. 1D illustrates the TEM image of NWs with uniform diameters. The HRTEM image was examined from one single NW, as shown in Fig. 1E. The regular spacing of the observed lattice planes is 0.237 nm, which is consistent with the separation of silver (111) planes. The SAED pattern of the NW indicates the single crystalline nature of silver, as seen in the set of Fig. 1E. The sets of spots marked with circle and rectangle respectively are indexed to the {111} and {220} planes of the sample respectively, which matches well with the face centered cubic silver phase (JCPDS File NO. 65-2871 from ASTM). Fig. 1F and G depict SEM images of the Ag NW film and the Ag NWs-PVA film laminated at a pressure of 30 MPa for 10 min. The average diameter of NWs increased from ~72 nm for Ag NW film to ~135 nm for Ag NWs-PVA film during the process of mechanical lamination.

Fig. 2A is XRD pattern of the composite film with transmittance of 85% at 550 nm. Four diffraction peaks labeled by red rectangles are observed at 38.07, 44.30, 64.48 and 77.42°, which can be assigned to the (111), (200), (220) and (311) reflections of face centered cubic structure of metallic silver (JCPDS File NO. 65-2871 from ASTM), respectively. The result was consistent with previous SAED measurement. The additional two peaks labeled by black rectangles are attributed to the PET substrate. No other peaks could be observed, indicating the absence of other impurities in the composite film. Fig. 2B shows the transmittance spectra of Ag NWs-PVA composite films with various densities of silver NWs. The samples were all laminated using a mechanical pressure of 30 MPa for 10 min. The composite film displays a specular transmittance from 93.4 to 66.3%, and a sheet resistance from 38.8 to 0.07 Ω/sq . Lower Ag NW concentration leads to a higher optical transmittance. Moreover, Ag NWs-PVA films with a lower density of Ag NWs exhibit a flat transmittance curve in the range of 400-700 nm. As the density of Ag NWs increased, the transmittances of composite films exhibit lower values in 400-550 nm than that in 550-700 nm range. This is due to the intense light scattering in short wavelength region.

We also characterized the optical haze of various concentrated composite films. The value of haze was determined as the degree of diffuse light scattering through the transparent films. It was calculated according to the relation $haze = (T_{tot} - T_{spec}) / T_{tot}$ by taking the substrate as the reference.

Where T_{tot} is the total transmittance, measured using the UV-Vis spectrophotometer with an integrating sphere; where T_{spec} is the specular transmittance of the film. There is a difference between T_{tot} and T_{spec} results from the light scattering of NWs. Fig. 2C depicts the optical haze versus the wavelength for a composite film with a light transmittance of 85%. The haze value is 10%, when the haze value from the ITO film on the glass is 2% (note Fig. S2). The inset of Fig. 2C is a plot of the optical haze of the films at 550 nm versus specular transmittance for various concentrated Ag NWs-PVA composite films laminated at a pressure of 30 MPa for 10 min. As can be seen, the haze values of the composite films decreased from 25.6% to 5.6%, while the transmittance increased from 64.1% to 90.3%. These results are very similar to those reported by Cui [28] and Han [41]. Very long Ag NWs are beneficial in reducing the optical haze of Ag NWs-based transparent films at a given transmittance.

Fig. 2D shows the relationship between the sheet resistance and transmittance of the Ag NW films and the Ag NWs-PVA composite films. The plot reveals that higher film transmittance results in lower sheet resistance, and the conductivity of the composite film is better than that of Ag NW film when they have similar optical transmittance. In general, to use a transparent conducting film in optoelectronic devices, it is required the transmittance of the film exceed 85% and the sheet resistance be less than 100 Ω /sq. The performance parameters of the films are required to be located in the area of green rectangular shadow, as shown in the bottom right corner of Fig. 2D. Thus it can be seen that the Ag NWs-PVA composite film is an excellent candidate for use as a transparent electrode. The plots in Fig. 2D indicate the transmittances of Ag NW films decreased slightly once Ag NW networks were transferred onto the PVA films to form the composite coatings. As previously discussed, the average diameters of Ag NWs are enlarged by the mechanical pressing, resulting in the reduction of inter-NWs spacing area and the decrease in the light transmittance of the composite film compared with the Ag NW film. In addition, the reduction of the transmittance varies with the density of the Ag NWs in the composite film. A higher density of NWs, causes a greater reduction in optical transmittance. This is because a higher concentration of Ag NWs reduces more area of inter-NWs spacing under same pressure.

It is very interesting to note that the laminated transparent film exhibits excellent electrical performance compared with the Ag NW film, demonstrating that the conductivity of the Ag

NWs-PVA composite film can be effectively improved by the lamination technique. We qualitatively measured the resistance of the Ag NW film and composite film using a digital multimeter. The resistance values of the Ag NW film varies from several to dozens of ohms if the distance between two multimeter probes is 0.1~0.2 cm. These values were dictated by the density of Ag NWs in the film. As the distance between the multimeter probes was increased, the resistance of the Ag NW film increased sharply, and even exceeded the capabilities of the multimeter measuring range of 20 M Ω . However, after laminating the Ag NW network onto the PVA film, the resistance of the composite film increased linearly as the distance between the two probes was extended. Fig. 3A shows the relative plots of the resistance versus distance between the multimeter probes for three representative composite films and the fitted linear relationships are indicated. The slopes of these plots were dependent on the photoelectrical performance of the composite films. Therefore, the characteristic of the conductivity of the two types of films is distinctly different.

To further evaluate the conducting uniformity of the conductive films, we calculated the standard deviation (SD) and standard error (SE) of the sheet resistance for the films (the formulas were shown in the supporting information). Using the Ag NW film with a transmittance of 86.5% and average sheet resistance of 120 Ω /sq as an example, after laminating the Ag NW network onto the PVA film at a pressure of 30 MPa for 10 min, the average sheet resistance of the composite film (85.1%) was sharply reduced to 0.67 Ω /sq. The calculated SD of the sheet resistance decreased from 127.5 to 0.12, the SE decreased from 42.5 to 0.04 and the percentage of SE was greatly reduced from 35.1% to 6.0%. Fig. 3B shows the sheet resistances with error bars for the Ag NW film and Ag NWs-PVA composite film. The resistance values were measured at nine representative points on the films. A reduced error bar of the sheet resistance for the composite film indicates that the uniformity of the conductivity is greatly improved, in comparison to the Ag NW film.

Thus it can be seen the conductivity and its uniformity of the Ag NW film are greatly improved after laminating with the PVA film. In NW networks, the electrons are transported via two paths. One is along one single NW, and the other is across the junctions of NWs by overcoming work function of metal. In our work, Ag NW film was fabricated by the spin-coating method, leading to the formation of random NW networks on the substrate. The electrical connections between Ag NWs are very weak since the NWs are poorly contacted to each other, as seen in the red dotted circles of Fig. 4A. Hence, overcoming the barrier of electronic transport between Ag NWs requires

a large amount of energy, yielding the poor conductivity exhibited by the Ag NW film. In the case of the Ag NWs with a length of several hundred micrometers, a long path of electronic transport in the network can be obtained. If two probes of the digital multimeter are placed close to measure the resistance of the Ag NW film, a low resistance measurement will result because the electrons are primarily transported along a single NW. As the distance between the two probes is increased, the electrons will move along one NW and across the junctions of NWs both, leading to the high resistance measurement for the Ag NW film.

After laminating Ag NW network onto the PVA film, Ag NWs were flattened and their average diameters were enlarged. The junctions of NWs are fused together due to mechanical pressing, as shown in the red dotted circles of Fig. 4B. This reveals that electrical channels of Ag NW network are established. The barrier of electronic transport between NWs is greatly decreased, leading to dramatic reduction of the contact resistance between NWs. There is an equal opportunity of electronic transport along one single NW and across the junctions of NWs. When we used the digital multimeter to measure the resistance of composite film, the values were proportional to the distance between the multimeter probes. This indicates that the composite film exhibits stable conductivity and a uniform resistance distribution over the whole area of the substrate.

AFM topography images of the Ag NW film and the Ag NWs-PVA composite film are shown in Fig. 5A and B. Fig. 5A displays that the height of the stacked Ag NWs above the substrate exceeds at least 300 nm, resulting in a high surface roughness for the conducting film, which is not compatible with high-efficiency optoelectrical devices. Following lamination of Ag NW network onto the PVA film, the surface roughness of the composite film was greatly reduced. The height variation of NWs above the substrate is just a few nanometers when using a laminating pressure of 30 MPa for 4 min, as displayed in Fig. 5B. The rough surface of the Ag NW film was smoothed because the protruding nanowires were flattened by mechanical laminating. The surface roughness of the composite film can be controlled by pressure and pressing time. However, a large pressure or a long pressing time could cause the Ag NWs be pressed into the PVA film to form grooves on the surface of composite film.

The effects of mechanical laminating time and intensity on the photoelectrical characteristics of Ag NWs-PVA composite film were also investigated in this work. Fig. 6A shows the sheet resistance of the composite film as a function of mechanical laminating time varied from 10 s to 60

min. The initial sheet resistance of Ag NW film was $\sim 124 \Omega/\text{sq}$. After applying a pressure of 30 MPa to the substrate, the conductivity of the composite film was rapidly improved. The sheet resistance of the composite film reduced to $24.92 \Omega/\text{sq}$ after a laminating time of 10 s. As the time was prolonged to 10 min, the sheet resistance of the film dropped to $0.56 \Omega/\text{sq}$. While the pressing time is further extended, the falling speed of sheet resistance slows down. Thus, it appears that a laminating time of 10 min causes the junctions of NWs effectively fuse together, establishing stable conductive network of Ag NWs. Surprisingly, the film exhibited a very low sheet resistance of $5.8 \text{ m}\Omega/\text{sq}$ if the pressing time was extends to 60 min.

Fig. 6B shows the transmittance of the Ag NW film and the Ag NWs-PVA film as a function of the mechanical laminating time varied from 10 s to 60 min. The initial transmittances of the Ag NW films were all about 85% at 550 nm and the transmittances of the composite films were 5% lower. The decreased transparency can be ascribed to the increased diameter of the Ag NWs and decreased area of the inter-NWs spacing in the network. However, the decrease in transmittance varies with the laminating time. The reduction in transmittance is relatively small if the films were laminated for a short time, less than 10 min. When the laminating time exceeded 10 min, the value of transmittance is almost constant. The increase in the diameter of NWs is relatively small with a short laminating time, leading to slight decline of the transmittance. The diameter of NWs will remain the same as the laminating time increased to more than 10 min, resulting in the stable transparency of the composite films.

Fig. 7A shows the sheet resistance of the composite film as a function of mechanical laminating pressure varied from 2 to 60 MPa. The initial sheet resistance of Ag NW film is $\sim 120 \Omega/\text{sq}$. After applying a mechanical pressure to the substrate, the sheet resistance of the composite film was decreased. The sheet resistance of composite film was $45 \Omega/\text{sq}$ with a laminating pressure of 2 MPa, and dropped to $1.07 \Omega/\text{sq}$ when the pressure was increased to 10 MPa. As the laminating pressure further increased, the decrease in sheet resistance becomes less. It is worth noting that the Ag NW film cannot be totally transferred onto the PVA film using a low pressure, less than 10 MPa, and the conductivity across the film is not uniform. However, the sheet resistance of the film exhibits a stable and uniform distribution as the laminating pressure enhanced to 30 MPa. This indicates that the laminating pressure of 30 MPa produces a stable conductive network of Ag NWs. When the laminating pressure is elevated to 60 MPa, the film exhibits a low resistance of $0.67 \Omega/\text{sq}$. But, the

composite film was deformed under such intense pressure.

Fig. 7B depicts the transmittance of the Ag NW film and the Ag NWs-PVA film as a function of the mechanical laminating pressure varied from 2 to 60 MPa. The initial transmittance of Ag NW films were all about 86% at 550 nm. The transmittance of composite films increased under a small pressure, because the NW network cannot be effectively transferred. As the laminating pressure enhanced, the Ag NW network was completely transferred onto the PVA film, and the average diameter of NWs was increased. Therefore, the area of inter-NWs spacing was gradually decreased, resulting in the continual reduction of the transmittance of composite films.

Thus, these results indicate that the laminating pressure is a more dominant factor than the laminating time to determine the enlargement of NW diameters, as well as the transmittance of the composite film.

As is well known, the brittleness of ITO films restricts its application as a flexible conductor. In order to apply the highly conducting Ag NWs-PVA composite film in flexible devices, we tested the mechanical stability of the composite film. The sheet resistance of the composite film after 300 bending cycles was measured and the variation in resistance versus cycle numbers is shown in Fig. 8A. For comparison, the left inset of Fig. 8A shows the resistance variations for ITO film on PET substrate under the same bending conditions. The right inset of Fig. 8A is the photography of the setup of cyclic bending test. The results reveal that the sheet resistance of the composite film shows less than 2% deviation after 300 bending cycles, while the resistance of ITO film sharply increases with an increase in bending cycles. The stable conductivity of Ag NWs-PVA film may be due to the formation of well-constructed electrical networks in the film. Thus, the composite film shows a high tolerance to bending and excellent mechanical stability.

To investigate the conductivity stability of the synthesized Ag NWs-PVA film, we compared the sheet resistances of the composite films freshly prepared, preserved for 90 and 180 days. The comparison histogram is shown in Fig. 8B. The effect of storing time on the conductivity of the films fabricated using a pressure of 10~60 MPa for 10 min was studied. After 90 days, the sheet resistances slightly increased for the most of samples, the largest enhancement ratio is 3.65 for the film laminated at 10 MPa pressure (The enhancement ratio is determined by the ratio of the difference in the sheet resistance of preserved and freshly prepared film to the sheet resistance of freshly prepared film. The increased ratios of the sheet resistance are listed in the Table S1). The

slight decline of the sheet resistance for one sample might be ascribed to a deviation of measurement. However, the composite films get larger increase of the sheet resistance in the next following 90 days. The enhancement ratio reaches 268.3 for the film with laminating pressure of 10 MPa. These results demonstrate that the composite films show better stability of the conductivity within 90 days of storage. In spite of the larger enhancement in the sheet resistance after 180 days, most of the composite films still are qualified for the transparent electrode due to their good electrical performance.

Moreover, it was also found that the sheet resistance of the composite films laminated using the pressure of 10 MPa rise the most quickly after storage. To investigate the effect of the laminating pressure on the conductivity stability of the films during storage, the films laminated at 10 MPa and 60 MPa pressure after 180 days of storage were characterized using XPS measurements. Fig. S3 shows the Ag 3d XPS spectra of the two samples, indicating the existence of silver species. To compare the oxidation degree of Ag NWs on the surface of two samples, we fitted the Ag3d XPS spectra of the samples. Two peaks at 374.0 and 373.6 eV can be assigned to Ag3d_{3/2} for Ag⁰ and Ag⁺, while 368.0 and 367.6 eV can be ascribed to Ag3d_{5/2} for Ag⁰ and Ag⁺ [42-45]. The fitted peak areas were used to determine the proportion of Ag⁰ and Ag⁺ in the silver species on the surface of the composite films. The proportion of Ag⁰ in the silver species was calculated by the ratio of the fitted peak area for Ag⁰ to the sum of the fitted peak areas of Ag⁰ and Ag⁺. In the case of the Ag 3d_{3/2}, the calculated proportions of Ag⁰ are 25.0% and 36.9% for the film laminated at 10 MPa and 60 MPa pressure. In case of Ag 3d_{5/2} they are 21.4% and 36.2%. These results show that the proportion of Ag⁰ is lower in the composite film that was laminated at a lower pressure. It can be concluded from this that the larger surface area of the Ag NWs was exposed to air, leading to the relatively ease of oxidation of the Ag and a decrease in the conductivity of the film. Thus, the mechanical laminating pressure is one of the vital factors determining the stability of conductivity in the composite film.

Finally, we tested the adhesion of the composite film using 3M Scotch tape. The Ag NW film on PET substrate was fairly easy to peel off and be scratched, demonstrating poor mechanical adhesion to the substrate. Whereas, the Ag NWs were hardly detached from the surface of composite film by the Scotch tape, as shown in Fig. S4. The improved adhesion can be mainly attributed to the compact contact between Ag NWs and PVA, which can effectively prevent

detaching the wires from the surface of composite film.

Conclusion

In conclusion, we have demonstrated a highly conductive, transparent electrode composed of the Ag NW network and the PVA film using a mechanical lamination technique. The flexible composite film exhibits excellent photoelectrical performance, low surface roughness, good mechanical and conducting stability, as well as improved adhesion to substrate. It is noted especially for its high electrical conductivity and stable, uniform conductivity distribution. These improved performances reveal the Ag NWs-PVA composite film is a promising candidate for use as a transparent conducting electrode in high-performance optoelectronic devices.

Acknowledgments

This work was supported by the National Natural Science Foundation of China (Grant No. 61307026) and Cultivation Fund for Outstanding Young Creative Talents in Higher Education of Guangdong Province (Grant No. 2013LYM_0091).

References

- 1 D. S. Hecht, L. B. Hu and G. Irvin, *Adv. Mater.*, 2011, 23, 1482-1513.
- 2 L. B. Hu, D. S. Hecht and G. Grüner, *Nanotechnology*, 2009, 20, 465304.
- 3 J. Lee, P. Lee, H. Lee, D. Lee, S. S. Lee and S. H. Ko, *Nanoscale*, 2012, 4, 6408-6414.
- 4 N. M. Kiasari, S. Soltanian, B. Gholamkhas and P. Servati, *RSC Adv.*, 2014, 4, 19663-19667.
- 5 S. H. Lee, S. S. Bhattacharyya, H. S. Jin and K. Jeong, *J. Mater. Chem.*, 2012, 22, 11893-11903.
- 6 W. Q. Fu, L. Liu, K. L. Jiang, Q. Q. Li and S. S. Fan, *Carbon*, 2010, 48, 1876-1879.
- 7 Y. Zhu, C. M. Hill and S. Pan, *Langmuir*, 2011, 27, 3121-3127.
- 8 L. Li, Z. B. Yu, W. Hu, C. Chang, Q. Chen and Q. B. Pei, *Adv. Mater.*, 2011, 23, 5563-5567.
- 9 M. W. Rowell and M. D. McGehee, *Energy Environ. Sci.*, 2011, 4, 131-134.
- 10 X. Fan, M. L. Zhang, X. D. Wang, F. H. Yang and X. M. Meng, *J. Mater. Chem. A*, 2013, 1, 8694-8709.
- 11 H. K. Park, S. W. Yoon, W. W. Chung, B. K. Min and Y. R. Do, *J. Mater. Chem. A*, 2013, 1, 5860-5867.

- 12 Y. Y. Kee, S. S. Tan, T. K. Yong, C. H. Nee, S. S. Yap, T. Y. Tou G. Sáfrán, Z. E. Horváth, J. P. Moscatello and Y. K. Yap, *Nanotechnology*, 2012, 23, 025706.
- 13 T. E. Williams, C. M. Chang, E. L. Rosen, G. Garcia, E. L. Runnerstrom, B. L. Williams, B. Koo, R. Buonsanti, D. J. Milliron and B. A. Helms, *J. Mater. Chem. C*, 2014, 2, 3328-3335.
- 14 D. R. Cairns, R. P. Witte, D. K. Sparacin, S. M. Sachsman D. C. Paine, G. P. Crawford and R. R. Newton, *Appl. Phys. Lett.*, 2000, 76, 1425.
- 15 H. K. Yu, S. Kim, B. Koo, G. H. Jung, B. Lee, J. Ham and J. Lee, *Nanoscale*, 2012, 4, 6831-6834.
- 16 B. F. Zhao, Z. C. He, X. P. Cheng, D. H. Qin, M. Yun, M. J. Wang, X. D. Huang, J. G. Wu, H. B. Wu and Y. Cao, *J. Mater. Chem. C*, 2014, 2, 5077-5082.
- 17 Y. J. Xia, K. Sun and J. Y. Ouyang, *Adv. Mater.*, 2012, 24, 2436-2440.
- 18 S. Ko, H. Choi, W. Lee, T. Kim, B. R. Lee, J. Jung, J. Jeong, M. H. Song, J. C. Lee, H. Y. Woo and J. Y. Kim, *Energy Environ. Sci.*, 2013, 6, 1949-1955.
- 19 T. Tokuno, M. Nogi, J. T. Jiu and K. Suganuma, *Nanoscale Res. Lett.*, 2012, 7, 281(p7).
- 20 R. C. Tenent, T. M. Barnes, J. D. Bergeson, A. J. Ferguson, B. To, L. M. Gedvilas, M. J. Heben and J. L. Blackburn, *Adv. Mater.*, 2009, 21, 3210-3216.
- 21 J. O. Hwang, J. S. Park, D. S. Choi, J. Y. Kim, S. H. Lee, K. E. Lee, Y. Kim, M. H. Song, S. Yoo and S. O. Kim, *ACS Nano*, 2012, 6, 159-167.
- 22 K. Rana, J. Singh and J. Ahn, *J. Mater. Chem. C*, 2014, 2, 2646-2656.
- 23 W. L. Hu, R. R. Wang, Y. F. Lu and Q. B. Pei, *J. Mater. Chem. C*, 2014, 2, 1298-1305.
- 24 Y. Cheng, S. L. Wang, R. R. Wang, J. Sun and L. Gao, *J. Mater. Chem. C*, 2014, 27, 5309-5316.
- 25 A. R. Rathmell, S. M. Bergin, Y. L. Hua, Z. Y. Li and B. J. Wiley, *Adv. Mater.*, 2010, 22, 3558-3563.
- 26 C. Wang, Y. J. Hu, C. M. Lieber and S. H. Sun, *J. Am. Chem. Soc.*, 2008, 130, 8902-8903.
- 27 A. L. Tiano, C. Koenigsmann, A. C. Santulli and S. S. Wong, *Chem. Commun.*, 2010, 46, 8093-8130.
- 28 L. B. Hu, H. S. Kim, J. Y. Lee, P. Peumans and Y. Cui, *ACS Nano*, 2010, 4, 2955-2963.
- 29 M. G. Kang, T. Xu, H. J. Park, X. G. Luo and L. J. Guo, *Adv. Mater.*, 2010, 22, 4378-4383.
- 30 W. Gaynor, J. Y. Lee and P. Peumans, *ACS Nano*, 2010, 4, 30-34.
- 31 X. Y. Zeng, Q. K. Zhang, R. M. Yu and C. Z. Lu, *Adv. Mater.*, 2010, 22, 4484-4488.

- 32 I. Chang, T. Park, J. Lee, M. H. Lee, S. H. Ko and S. W. Cha, *J. Mater. Chem. A*, 2013, 1, 8541-8546.
- 33 I. Chang, T. Park, J. Lee, H. B. Lee, S. Ji, M. H. Lee, S. H. Ko and S. W. Cha, *Int. J. Hydrogen energy*, 2014, 39, 7422-7427.
- 34 P. Lee, J. Lee, H. Lee, J. Yeo, S. Hong, K. H. Nam, D. Lee, S. S. Lee and S. H. Ko, *Adv. Mater.*, 2012, 24, 3326-3332.
- 35 P. Lee, J. Ham, J. Lee, S. Hong, S. Han, Y. D. Suh, S. E. Lee, J. Yeo, S. S. Lee, D. Lee and S. H. Ko, *Adv. Funct. Mater.*, 2014, DOI: 10.1002/adfm.201400972.
- 36 J. H. Lee, P. Lee, D. Lee, S. S. Lee and S. H. Ko, *Cryst. Growth Des.*, 2012, 12, 5598-5605.
- 37 J. Y. Lee, S. T. Connor, Y. Cui and P. Peumans, *Nano Lett.*, 2008, 8, 689-692.
- 38 W. Gaynor, G. F. Burkhard, M. D. McGehee and P. Peumans, *Adv. Mater.*, 2011, 23, 2905-2910.
- 39 S. Han, S. Hong, J. Ham, J. Yeo, J. Lee, B. Kang, P. Lee, J. Kwon, S. S. Lee, M. Y. Yang and S. H. Ko, *Adv. Mater.*, 2014, DOI: 10.1002/adma.201400474.
- 40 J. Lee, P. Lee, H. B. Lee, S. Hong, I. Lee, J. Yeo, S. S. Lee, T. S. Kim, D. Lee and S. H. Ko, *Adv. Funct. Mater.*, 2013, 23, 4171-4176.
- 41 T. Kim, A. Canlier, G. H. Kim, J. Choi, M. Park and S. M. Han, *ACS App. Mater. Interfaces*, 2013, 5, 788-794.
- 42 N. H. Turner and J. A. Schreifels, *Anal. Chem.*, 2000, 72, 99R-110R.
- 43 C. Hu, Y. Q. Lan, J. H. Qu, X. X. Hu and A. M. Wang, *J. Phys. Chem. B*, 2006, 110, 4066-4072.
- 44 H. Zhang, Q. Fu, Y. X. Yao, Z. Zhang, T. Ma, D. L. Tan and X. H. Bao, *Langmuir*, 2008, 24, 10874-10878.
- 45 M. I. Mejía, G. Restrepo, J. M. Marín, R. Sanjines, C. Pulgarín, E. Mielczarski, J. Mielczarski and J. Kiwi, *ACS App. Mater. Interfaces*, 2010, 2, 230-235.

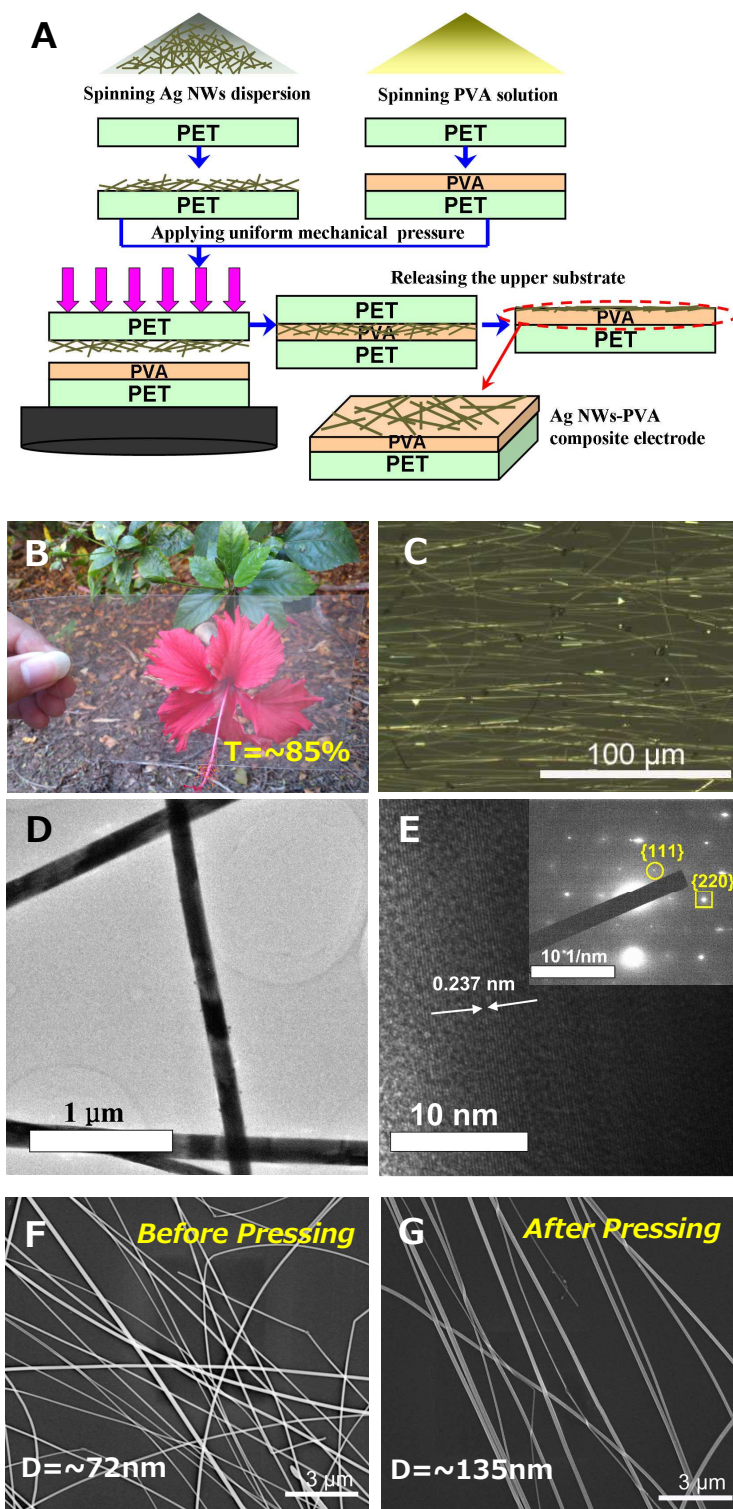


Fig. 1 (A) Schematic illustration of the fabrication procedure of Ag NWs-PVA composite film; (B) Photography of and (C) optical micrograph of a composite film with transmittance of 85% at 550 nm; (D) TEM image of the Ag NWs; (E) HRTEM image of one Ag NW; the fringe spacing (0.237

nm) observed in this image corresponds to the separation between the (111) lattice planes; the inset is SAED pattern of the Ag NW. (F) SEM images of the Ag NWs film and (G) the Ag NWs-PVA composite film on the PET substrate.

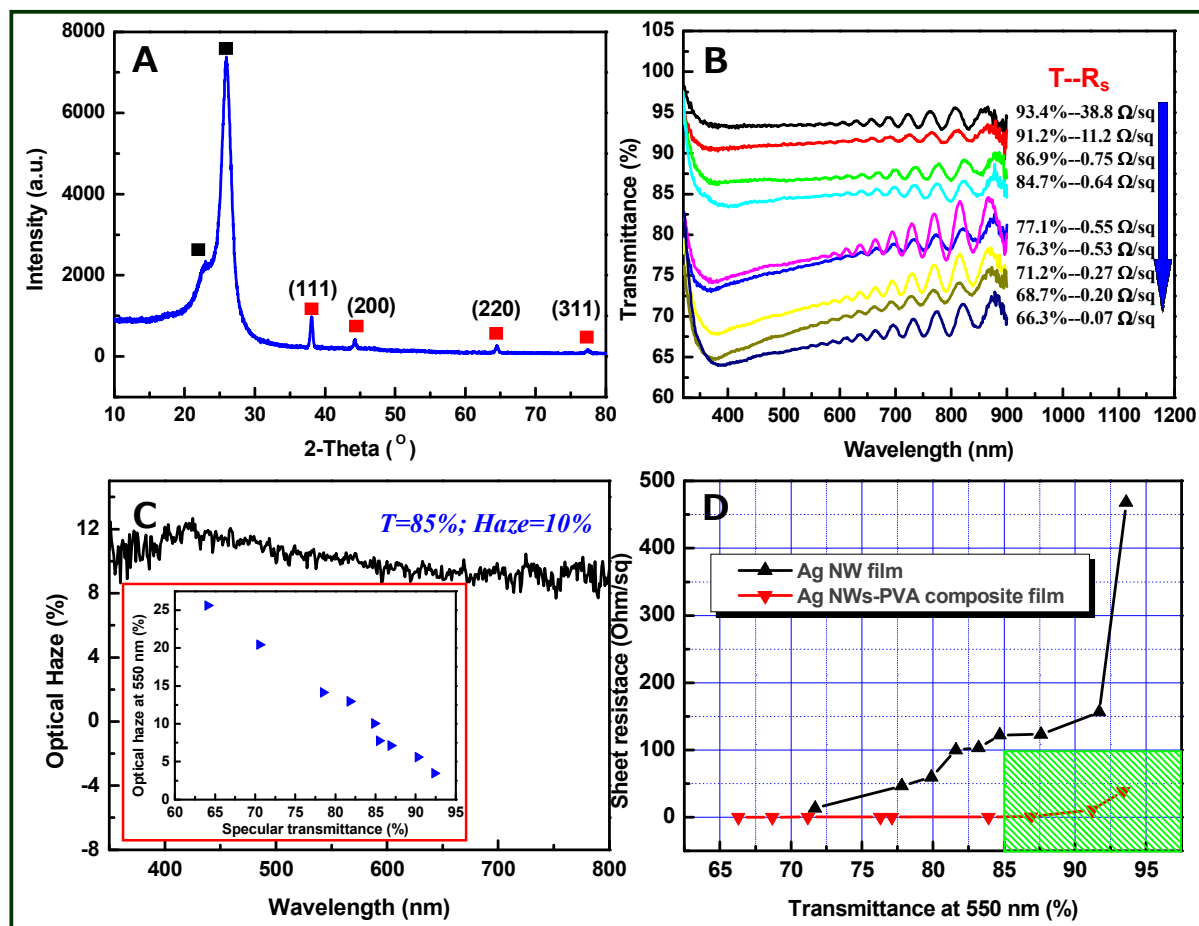


Fig. 2 (A) XRD pattern of the composite film with transmittance of 85% at 550 nm; (B) Optical transmittance spectra of various concentrated Ag NWs-PVA composite films laminated at 30 MPa pressure for 10 min; (C) Optical haze *versus* wavelength for a composite film with a transmittance of 85% at 550 nm; the inset of Fig. 2C is a plot of the optical haze at 550 nm *versus* specular transmittance of various concentrated Ag NWs-PVA composite films laminated at 30 MPa pressure for 10 min; (D) Relative plots of sheet resistance *versus* specular transmittance of the Ag NW films and the Ag NWs-PVA composite films laminated at 30 MPa pressure for 10 min; the photoelectrical performance parameters of the Ag NW films and the Ag NWs-PVA composite film are labeled by black triangles and red inverted triangles, respectively.

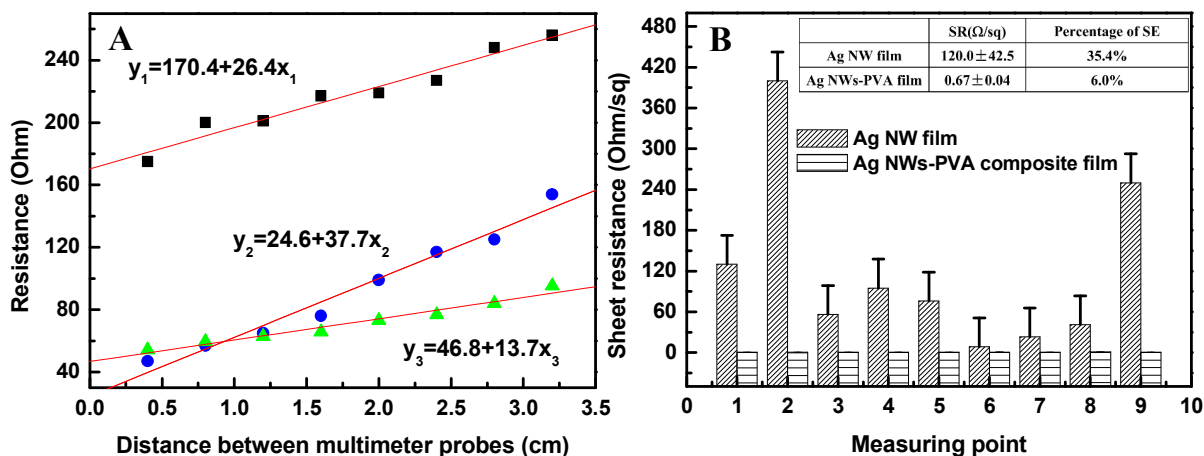


Fig. 3 (A) Relative plots of the resistance versus distance between the multimeter probes (The resistance values were measured using a digital multimeter). The fitted linear relationships were given. (B) The sheet resistances with error bars of Ag NW film and Ag NWs-PVA composite film, measured at nine representative points; the inset is a table presented the values of SR (sheet resistance) and the percentage of SE for Ag NW film and Ag NWs-PVA composite film.

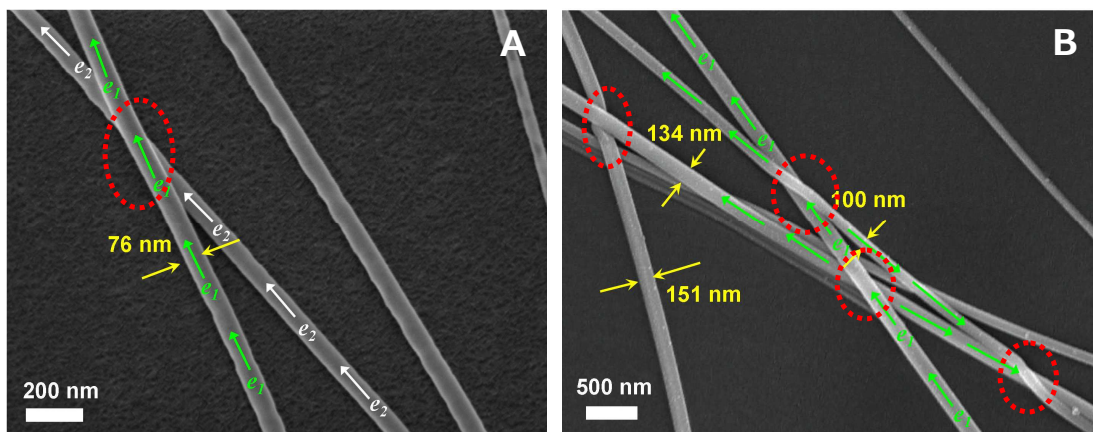


Fig. 4 SEM images of the Ag NW film (A) and the Ag NWs-PVA composite film (B). The junctions of NWs were marked by red dotted circles, and the scale bar respectively is 200 and 500 nm. The arrows represent the transport of the electrons in NWs.

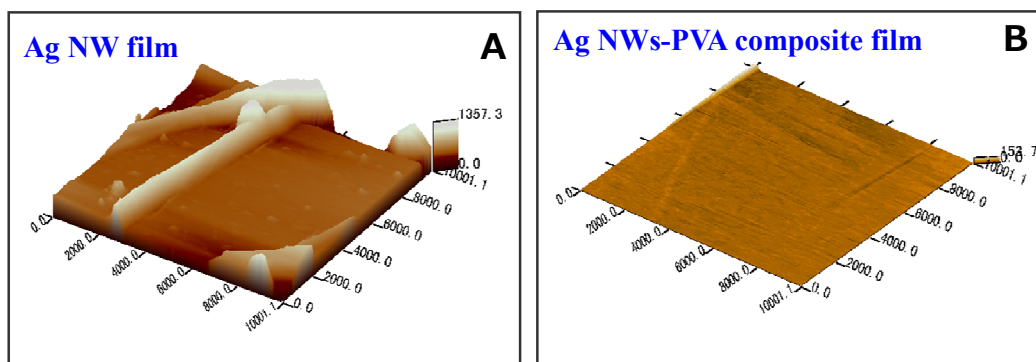


Fig. 5 AFM topography images of the Ag NW film (A) and the Ag NWs-PVA composite film laminated at a mechanical pressure of 30MPa for 4 min (B). The scale range is $10\ \mu\text{m}\times 10\ \mu\text{m}$.

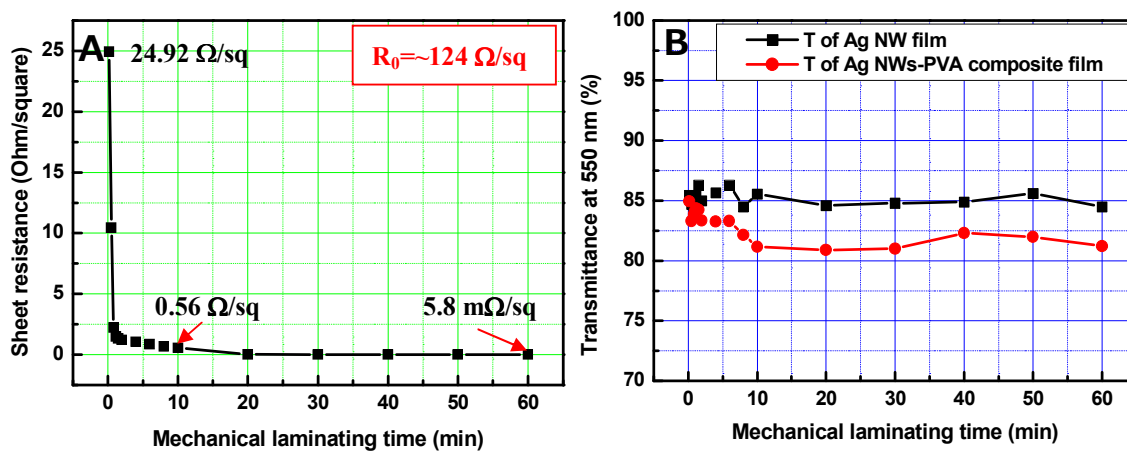


Fig. 6 Electrical and optical characterizations of the Ag NWs-PVA composite films laminated at a pressure of 30 MPa for 10s to 60 min; the initial sheet resistance of the Ag NW film is $\sim 124 \Omega/\text{sq}$. (A) Relative plots of the sheet resistance *versus* the mechanical laminating time. (B) Relative plots of the transmittance at 550 nm *versus* the mechanical laminating time. The black squares and the red circles represent the transmittance of Ag NW films and Ag NWs-PVA films, respectively.

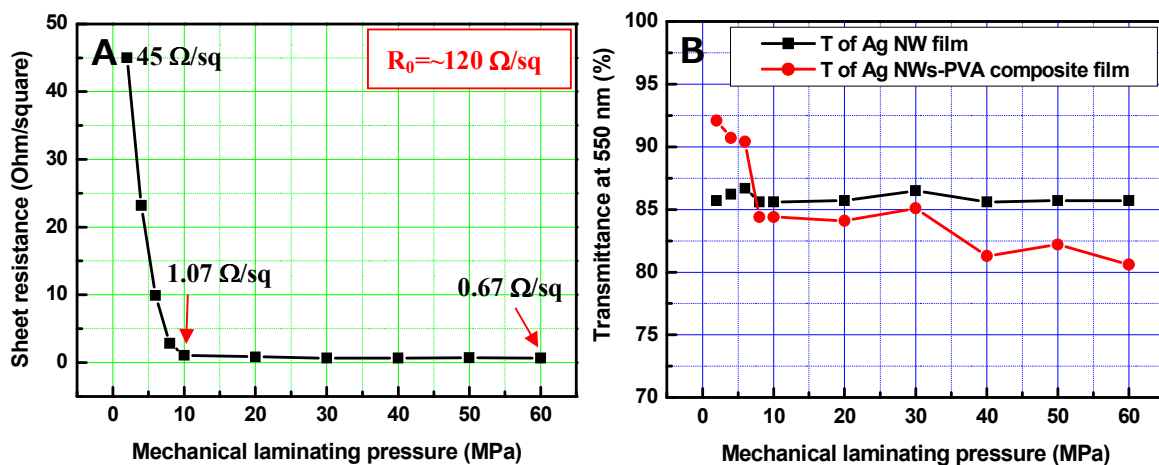


Fig. 7 Electrical and optical characterizations of the Ag NWs-PVA composite film laminated at pressure from 2 to 60 MPa for 10 min; the initial sheet resistance of the Ag NW film is $\sim 120 \Omega/\text{sq}$. (A) Relative plots of the sheet resistance *versus* the mechanical laminating pressure. (B) Relative plots of the transmittance at 550 nm *versus* the mechanical laminating pressure. The black squares and the red circles represent the transmittance of Ag NW films and Ag NWs-PVA films, respectively.

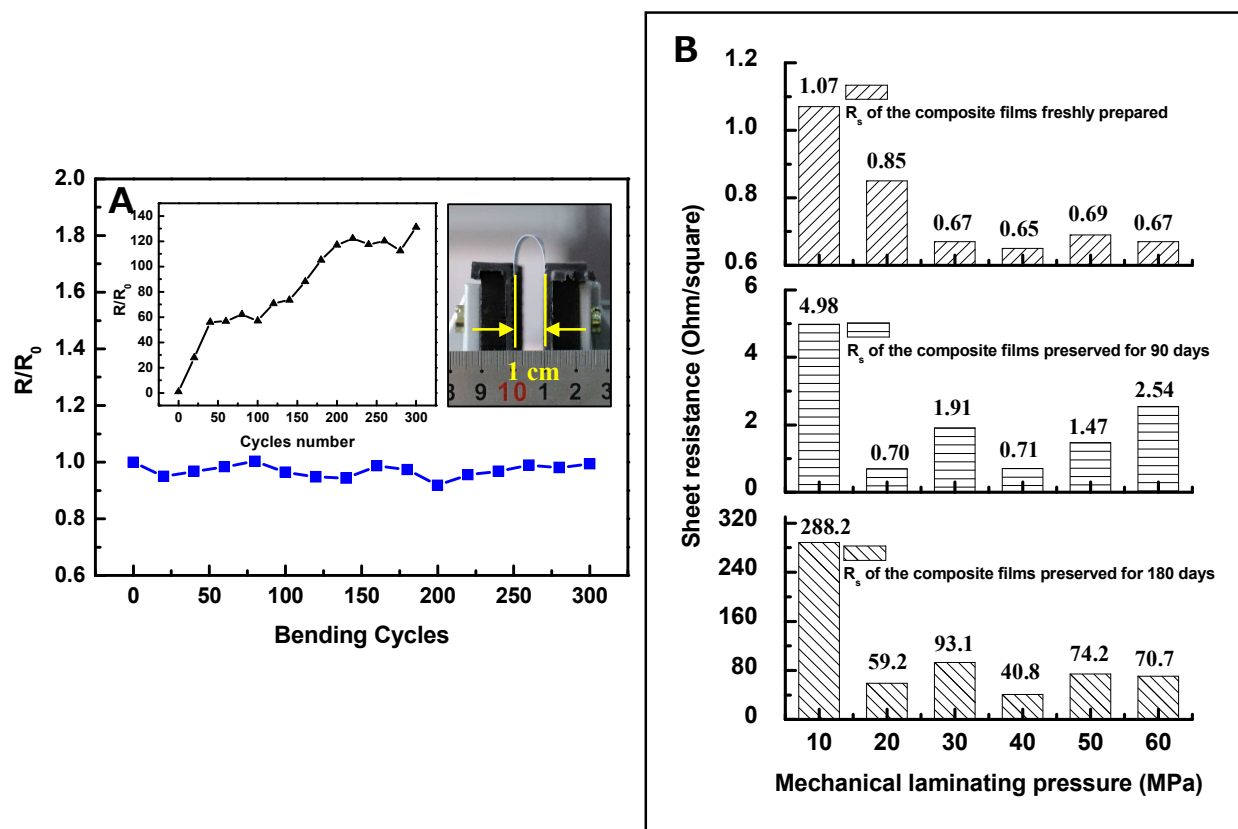
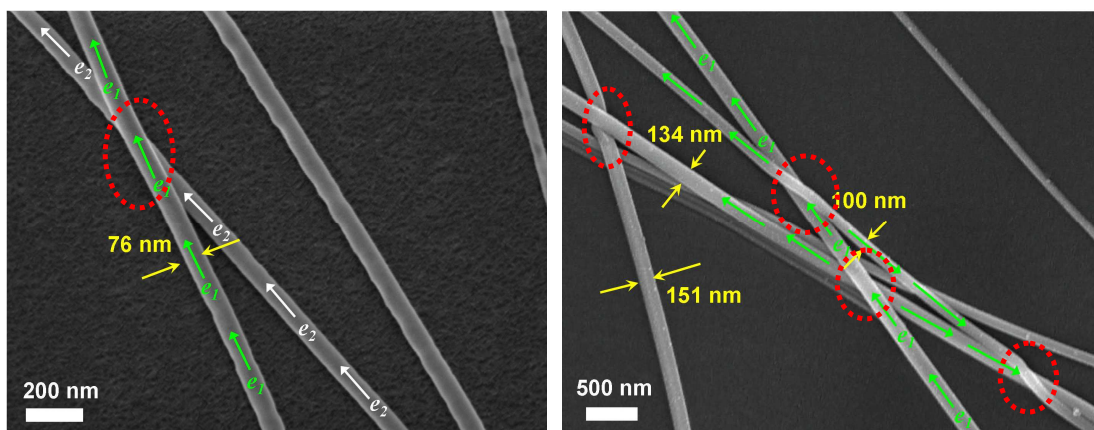


Fig. 8 (A) Variations in resistance of Ag NWs-PVA composite film *versus* bending cycles; the left inset is variations in resistance of ITO film on PET substrate *versus* bending cycles, and the right inset is the photography of the setup of cyclic bending test; the area of film is 3×3 cm. (B) The histogram of the sheet resistances for the composite film freshly prepared, preserved for 90 and 180 days. The sheet resistances of the composite film were shown in the histogram, and the unit of the numbers is Ω/sq .



(Left) SEM images of the Ag NW film; (Right) SEM images of the Ag NWs-PVA composite film. The connections of the NWs were fused together after laminating Ag NW network onto the PVA film, and electrical networks were established. Green and white arrows represent the transport of the electrons in NWs.